Journal of Molecular Liquids 367 (2022) 120472

Contents lists available at ScienceDirect

Journal of Molecular Liquids

journal homepage: www.elsevier.com/locate/molliq

Machine learning for predicting the solubility of high-GWP fluorinated refrigerants in ionic liquids

Salvador Asensio-Delgado, Fernando Pardo, Gabriel Zarca, Ane Urtiaga *

Department of Chemical and Biomolecular Engineering, Universidad de Cantabria. Av. Los Castros 46, Santander 39005, Spain

ARTICLE INFO

Article history:
Received 30 May 2022
Revised 12 September 2022
Accepted 22 September 2022
Available online 28 September 2022

Keywords:
Artificial neural network
Ionic liquids
Refrigerant gases
Predictive tool
GWP mitigation

ABSTRACT

The development of technology to reduce the environmental impact of fluorinated refrigerant gases (F-gases) is currently of outmost importance. The capture of F-gases in ionic liquids (ILs) is envisaged as solution to avoid emissions of F-gases to the atmosphere, and many studies have been devoted to the experimental determination of the vapor-liquid equilibrium of F-gas/IL mixtures. However, this is an expensive and time-consuming task, so finding prescreening options that can reduce the experimental load would pose a significant advantage in the development of new industrial-scale processes. Here, we develop a prescreening tool based on the use of artificial neural networks (ANNs) to predict the solubility of F-gases in ILs from easily accessible properties of the pure compounds, such as the critical properties of the gases or the molar mass and volume of the IL. We have used the UC-RAIL database with more than 4300 solubility data of 24 F-gases in 52 ILs. The ANN resulting from this study is capable to predict the fed dataset with an average absolute relative deviation (AARD) and mean absolute error (MAE) of 10.93% and 0.014, respectively, and we further demonstrate its predictive capabilities showing the very accurate prediction of a system including R-1243zf, an F-gas that was not present in the training set because it had not been previously studied. Finally, the developed ANN is implemented in an easy-to-use spreadsheet that will allow to extend its use in the prescreening of ILs towards the abatement and recovery of high environmental impact refrigerant gases.

1. Introduction

Refrigeration is considered one the greatest engineering achievements of the 20th century, with applications that span from the preservation of fresh food and pharmaceutical compounds to providing air conditioning comfort in domestic, industrial, and transport environments [1]. Currently, a majority of refrigeration and air conditioning (RAC) equipment apply compression assisted evaporation and condensation cycles that use hydrofluorocarbons (HFCs) as refrigeration fluids. HFCs are synthetic fluorinated gases that were created to substitute the ozone-depleting chlorofluorocarbons (CFCs) and hydrochlorofluorocarbons (HCFCs) previously applied. However, HFCs are still powerful greenhouse gases. At present, a new class of related compounds, the hydrofluoroolefins (HFOs), with very low global warming potential (GWP), are gaining market share as a strategy for climate change mitigation [2]. As a result, commercial refrigerant blends are transitioning from HFC-only to low-GWP HFC/HFO mixtures containing mainly the HFCs R-32 (difluoromethane) and R-134a (1,1,1,2-tetrafluoroethane), and the HFOs R-1234yf (2,3,3,3-tetrafluoropropene) and R-1234ze(E) (trans-1,3,3,3-tetrafluoropropene) [3].

The emissions of HFCs contributed to global greenhouse gas emissions as 0.73 and 1.1 Gt CO_2-eq in 2010 and 2015, respectively, and only a small fraction of the HFCs in waste equipment are recovered or sent to incineration [4]. New regulations aim to stop this steady-rise scenario, among which the Kigali Amendment (2016) to the Montreal Protocol stands out, by defining a schedule for phasing down the production and consumption of HFCs by 85% by the late 2040s [5–7]. Thus, apart from the search for new low-GWP working fluids [8,9], the current context presents the opportunity of creating new abatement and regeneration technologies to recover and purify the HFCs from waste refrigerant mixtures, allowing their reuse in the formulation of the new HFC/HFO blends. Additionally, some mid-GWP HFC/HFO blends will only be used in the interim between emission reduction steps in international F-gas regulations, so recovering the HFOs to reuse them in low-GWP blends is of the utmost interest [10].

Different technologies have been proposed to perform the recovery of refrigerants from mixtures that usually exhibit azeotropic or near-azeotropic behavior [10]. These are, namely, membrane separation [11–15], adsorption on porous materials [16–

* Corresponding author.
E-mail address: urtiaga@unican.es (A. Urtiaga).

https://doi.org/10.1016/j.molliq.2022.120472
0167-7322/

18], and absorption-based extractive distillation processes [19–21], in which ionic liquids (ILs) have attracted the most attention as entrainers. ILs are compounds preferentially composed of bulky organic ions that are liquid near room temperature [22] and exhibit unique properties, namely, nonvolatility, nonflammability, existence in liquid state over a wide range of temperatures, chemical and thermal stability, and ability to solubilize both polar and nonpolar compounds [23]. In particular, the high solubility of HFCs in ILs is related to hydrogen bonding and polar interactions between the solute and solvent molecules in the liquid mixture, and to favorable entropic effects in ILs featuring large free volume [24].

For developing F-gas reclamation processes, ILs need to be tested to find those that preferentially absorb some refrigerants over others, providing high solubility selectivity. In this regard, imidazolium ILs with thiocyanate and dicyanamide anions [23,25], as well as the combination of these anions with pyridinium cations [26], have shown high solubility selectivity for key F-gas separations, which can be related to the small molar volume and no fluorination of the anions [10]. In addition, the favorable solubility of HFCs and HFOs in ILs is encouraging the design of more energy efficient absorption refrigeration systems, in which the gas compressor is substituted by an absorber and a desorber [27]. In this field, the interest lies in finding low-viscosity ILs capable of dissolving large quantities of refrigerant gases of low-GWP so as to reduce the amount of solvent used and minimize the pumping costs.

In any case, knowledge on the vapor-liquid equilibrium (VLE) at several temperatures and pressures is crucial for the development of both applications. However, the experimental VLE determination is expensive and time-consuming and there are so many different fluorinated refrigerants, and even more possible ILs, that testing all the combinations becomes an unattainable goal. For this reason, developing a screening tool that allows the user to test the solubility behavior of F-gases in different ILs has a great interest, including systems for which there are not experimental information available [26].

In this sense, artificial intelligence approaches have shown excellent prediction capability in the field of chemical and process engineering, including their use in the design of new more sustainable refrigerants (HFCs, HFOs, and HCFOs) [28]. Machine learning are superior versus classical data analysis techniques in two main aspects, data classification and prediction; consequently, their predictive ability is being investigated in depth in ILs research [29]. For example, an Artificial Neural Network (ANN) and a Supported-Vector Machine (SVM) were trained to predict the viscosity of ILs using 1079 experimental data points from 45 ILs [30], and the melting point of ILs was predicted using a SVM trained using 22268 data points of 2068 ILs [31]. Some studies also developed machine learning methods to predict the solubility in ILs of CO_2 [32–36] and H_2S [36–38], where ANNs showed improved prediction accuracy compared to cubic equations of state. In the field of refrigerant gases, previous attempts of developing ANNs to predict their solubility in ILs are limited to the works of Faúndez et al. [39], who used 254 data points of the solubility of the R-32 refrigerant in different ILs to train an ANN, and later extended the database to 642 data points to include one- and two-carbons HFCs [40]. However, training machine learning tools is not straightforward and requires strategies to overcome the difficulty in finding a global minimum, avoid overfitting and obtain a meaningfully predictive model [41]. As it will be detailed in section 2, several approaches are applied in this work to overcome these shortcomings, namely, applying multi-start initialization, using early-stopping methods to avoid overfitting, and using a large dataset as input for the training.

In this work, we use the recently published UC-RAIL database containing over 4000 solubility data of 24 fluorinated refrigerant gases (F-gases) in 52 ILs [10] to train an ANN to predict the molar fraction of F-gas absorbed from pure component data, namely, critical properties and vapor pressure of the gas, molecular weights and number of fluorine atoms of the gas and the IL, and IL density. We have trained the ANN with different F-gas families that include HFCs, HFOs, hydrochlorofluoroolefins (HCFOs), CFCs, HCFCs, and perfluorocarbons (PFCs). Furthermore, the trained ANN has been used to predict recently published VLE data that were not included in the UC-RAIL database. The ANN also describes the phase behavior at several pressures and temperatures. The developed tool will be useful in the initial stages of F-gas capture processes to make fast screenings of several ILs.

2. Methodology

2.1. Dataset

The VLE data recently compiled in the UC-RAIL database were used for developing the ANN to predict the solubility of fluorinated refrigerant gases in ILs [10]. This database contains experimental data for the solubility of 24 F-gases in 52 ILs that were randomly divided in training, validation, and test sets in the proportion 70/15/15. Out of the 4444 experimental data points available, 1% of the information (48 points) was removed. These points correspond to the solubility of fluorobutenes in ILs, for which there are not enough data available to make a meaningful network training, and to F-gas/IL systems that deal with the solubility of R-134a in [C_2mim][Ac] and R-125 in [C_2mim][Ac], [C_4mim][Ac], and [C_6mim][Cl]. The latter four systems could not be predicted accurately, even if they were purposely included in the training set. This can be considered a new proof of the unexpectedly strong interactions found between carboxylate and chloride anions with R-134a and R-125 gases [42,43]. As reported by Morais et al. [42], these interactions could be of chemical nature, like those of CO_2 absorption [44]. The list of IL cations and anions and F-gases considered in this work is presented in Table 1.

2.2. Artificial neural networks

An ANN is formed by processing units called neurons that are organized in layers [45]. The first layer of the network is the input layer, through which the input data is fed to the ANN. The input data provides useful and relevant information, the so-called features, to the network. These features are then fed to the hidden layers, where they undergo a series of transformations. Next, the information is sent from the last hidden layer to the output layer, which provides the results [46,47]. Each of the hidden layers communicates with their adjacent layers, this is, the ones that are immediately before and after. To that end, each neuron j in layer i receives k inputs ($u_{i-1,k}$) from the previous layer (k is the number of neurons in the previous layer), multiplies them by their corresponding weights (w_{ijk}) and adds the bias (b_{ij}):

$$y_{ij} = b_{ij} + \sum_k w_{ijk} u_{i-1,k} \tag{1}$$

The calculated value of each neuron (y_{ij}), normalized with a transfer function, represents the input to the neurons of the next layer. In this work, we have used the hyperbolic tangent sigmoid function (*tansig*) to normalize the neuron output [48]:

$$u_{ij} = \frac{2}{1 + \exp\left(-2y_{ij}\right)} - 1 \tag{2}$$

where u_{ij} is the normalized neuron output which will be used as an input for the following layer.

Table 1
List of IL cations and anions and F-gases included in the UC-RAIL database.

Ionic Liquids			
Cation	**Cation name**	**Anion**	**Anion name**
$[C_2mim]^+$	1-ethyl-3-methylimidazolium	$[Ac]^-$	acetate
$[C_4mim]^+$	1-butyl-3-methylimidazolium	$[BEI]^-$	bis(pentafluoroethylsulfonyl)imide
$[C_6mim]^+$	1-hexyl-3-methylimidazolium	$[BF_4]^-$	tetrafluoroborate
$[C_7mim]^+$	1-heptyl-3-methylimidazolium	$[Cl]^-$	chloride
$[C_8mim]^+$	3-octyl-1-methylimidazolium	$[Et_2PO_4]^-$	diethylphosphate
$[(C_8)_2im]^+$	1,3-dioctylimidazolium	$[FEP]^-$	tris(pentafluoroethyl)trifluorophosphate
$[C_8H_4F_{13}mim]^+$	1-(3,3,4,4,5,5,6,6,7,7,8,8,8-tridecafluorooctyl)-3-methylimidazolium	$[FS]^-$	2-(1,2,2,2-tetrafluoroethoxy)-1,1,2,2-tetrafluoroethanesulfonate
		$[HFPS]^-$	1,1,2,3,3,3-hexafluoropropanesulfonate
$[C_{12}mim]^+$	1-dodecyl-3-methylimidazolium	$[I]^-$	iodide
$[(C_1)_2C_3im]^+$	1,2-dimethyl-3-propylimidazolium	$[MeSO_4]^-$	methylsulfate
		$[OTf]^-$	trifluoromethanesulfonate
$[C_2mpy]^+$	1-ethyl-3-methylpyridinium	$[Pe]^-$	pentanoate
$[C_3mpy]^+$	3-methyl-1-propylpyridinium	$[PF_6]^-$	hexafluorophosphate
$[C_4mpy]^+$	1-butyl-3-methylpyridinium	$[Pr]^-$	propionate
$[P_{4441}]^+$	tributyl(methyl)phosphonium	$[PFBS]^-$	perfluorobutanesulfonate
$[P_{4442}]^+$	tributyl(ethyl)phosphonium	$[PFP]^-$	perfluoropentanoate
$[P_{44414}]^+$	tributyl(tetradecyl)phosphonium	$[SCN]^-$	thiocyanate
$[P_{66614}]^+$	trihexyl(tetradecyl)phosphonium	$[Tf_2N]^-$	bis(trifluoromethylsulfonyl)imide
$[m\text{-}2\text{-}HEA]^+$	*N*-methyl-2-hydroxyethylammonium	$[TFES]^-$	1,1,2,2-tetrafluoroethanesulfonate
		$[TMeM]^-$	tris(trifluoromethylsulfonyl)methide
		$[TMPP]^-$	bis(2,4,4-trimethylpentyl)phosphinate
		$[TPES]^-$	1,1,2-trifluoro-2-(perfluoroethoxy)ethanesulfonate
		$[TTES]^-$	1,1,2-trifluoro-2-(trifluoromethoxy)ethanesulfonate

Fluorinated refrigerants			
HFCs	**Chemical name**	**HFOs/ HCFOS**	**Chemical name**
R-41	fluoromethane	R-1234yf	2,3,3,3-tetrafluoropropene
R-32	difluoromethane	R-1234ze(E)	trans-1,3,3,3-tetrafluoropropene
R-23	trifluoromethane	R-1233zd(E)	trans-1-chloro-3,3,3-trifluoropropene
R-161	fluoroethane	R-1243zf	3,3,3-trifluoropropene
R-152a	1,1-difluoroethane	**PFCs**	**Chemical name**
R-143a	1,1,1-trifluoroethane	R-14	tetrafluoromethane
R-134	1,1,2,2-tetrafluoroethane	R-116	hexafluoroethane
R-134a	1,1,1,2-tetrafluoroethane	R-218	octafluoropropane
R-125	pentafluoroethane	**Phased out**	**Chemical name**
R-245fa	1,1,1,3,3-pentafluoropropane	R-114	1,2-dichloro-1,1,2,2-tetrafluoroethane
R-236fa	1,1,1,3,3,3-hexafluoropropane	R-114a	1,1-dichloro-1,2,2,2-tetrafluoroethane
R-227ea	1,1,1,2,3,3,3-heptafluoropropane	R-124	2-chloro-1,1,1,2-tetrafluoroethane
		R-124a	2-chloro-1,1,2,2-tetrafluoroethane
		R-22	chlorodifluoromethane
		R-22B1	bromodifluoromethane

After the last hidden layer, the normalized outputs are multiplied by the output layer weights and summed using the *purelin* function [48]. A developed explanation of the ANN calculation can be found in the Supplementary Material.

To develop the ANN, all the weights, w_{ijk}, and biases, b_{ij}, are parametrized for every neuron in every layer. Unfortunately, there is not an explicit rule that determines the number of hidden layers or the number of neurons in each layer, so they must be selected by trial and error [39]. In this work, we focused in three-hidden-layers structures containing between 1 and 10 neurons in each layer. This decision was made after checking that the structures containing only one or two hidden layers resulted in much worse performances. For each possible combination, 50 different networks were trained to overcome the main shortcoming of the ANN regarding initialization and only the best one was kept. The training was made using the Neural Network Toolbox of MATLAB R2021a software using the BFGS Quasi-Newton training function (*trainbfg*). The maximum number of epochs was set to 10000, but the maximum number of fails was kept at 50 to avoid overfitting, so that the final network was only trained for 1544 epochs.

We used the average absolute relative deviation (AARD) as the performance function, Eq. (3), because minimizing the AARD allowed the accurate prediction of the solubility of low-sorbing gases, while it also provided low absolute errors for the prediction of highly soluble gases. However, the root mean square error (RMSE) and mean absolute error (MAE) were also evaluated as performance indicators of the ANN.

$$\begin{aligned} AARD &= \frac{100}{N}\sum_i \left|\frac{x_{calc,i}-x_{exp,i}}{x_{exp,i}}\right| \\ RMSE &= \sqrt{\frac{1}{N}\sum_i \left(x_{calc,i}-x_{exp,i}\right)^2} \\ MAE &= \frac{1}{N}\sum_i \left|x_{calc,i}-x_{exp,i}\right| \end{aligned} \tag{3}$$

3. Results

3.1. Feature selection

The ANN was trained to predict the solubility of F-gases in ILs as a function of the equilibrium temperature and pressure using easily accessible and well-known properties of the pure solvents and solutes. The properties used to describe the IL solvents are the molar mass of the cation and the anion (M_{cat} and M_{an}), the IL molar volume (Vm_{IL}), and the number of fluorine atoms in the IL ($F_{at,IL}$). The selection of these properties was based on our previous review on the topic [10], where we showed that all of them had a

relevant effect on the solubility of F-gases in ILs. For the F-gases, we used as features the critical properties of pressure, temperature, and volume (T_c, P_c, and V_c), the acentric factor (ω), the vapor pressure (P_{vap}), the molar mass (M_{gas}), and the number of fluorine atoms ($F_{at,gas}$). The thermophysical properties database and equations of state library Coolprop 6.4.0 [49] was used to calculate the vapor pressures of all the compounds available and the rest were calculated using the correlations available in the book by Poling and Prausnitz [50]. The input properties for each IL and F-gas are compiled in the Supplementary Material.

Fig. 1a presents the correlation coefficients of the selected input variables with the molar fraction of gas absorbed (x). The numeric values of the correlation coefficients as well as the regression lines and individual histograms for the variables are presented in Figure S1 in the Supplementary Information. As can be observed, the correlation coefficient between each descriptor and the solubility (x), that can be read in the bottom line of Fig. 1a, are lower than ±0.25, except for the equilibrium temperature, T, and the refrigerant critical pressure, P_c. These moderate correlation coefficients indicate that all of them should have a very similar importance on the solubility prediction. Among the IL features, the anion molar mass, M_{an}, presents the best correlation to the solubility (x) with a correlation coefficient of 0.23. Additionally, Fig. 1a also provides information regarding the positive or negative correlation between the descriptor variables. For instance, the molar mass of the gas (M_{gas}), is positively correlated with its critical molar volume (V_c), and degree of fluorination ($F_{at,gas}$), as the most fluorinated gases are bigger and have higher molar mass than those hydrofluorocarbon gases with more hydrogen atoms than fluorine atoms bonded to the carbon chain. In addition, it is possible to infer whether there is a significant contribution of one input variable on the prediction of the output variable by assessing its fractional variance, which is calculated as the variance of each variable over the cumulative variance of all the input variables [51]. Thus, Fig. 1b shows the fractional variance of each of the descriptors of the ILs and F-gases, which ranges between 5 and 15% of the total cumulative variance in all cases. Therefore, we can infer that all the input variables have a similar importance in the prediction of F-gas solubility *a priori*.

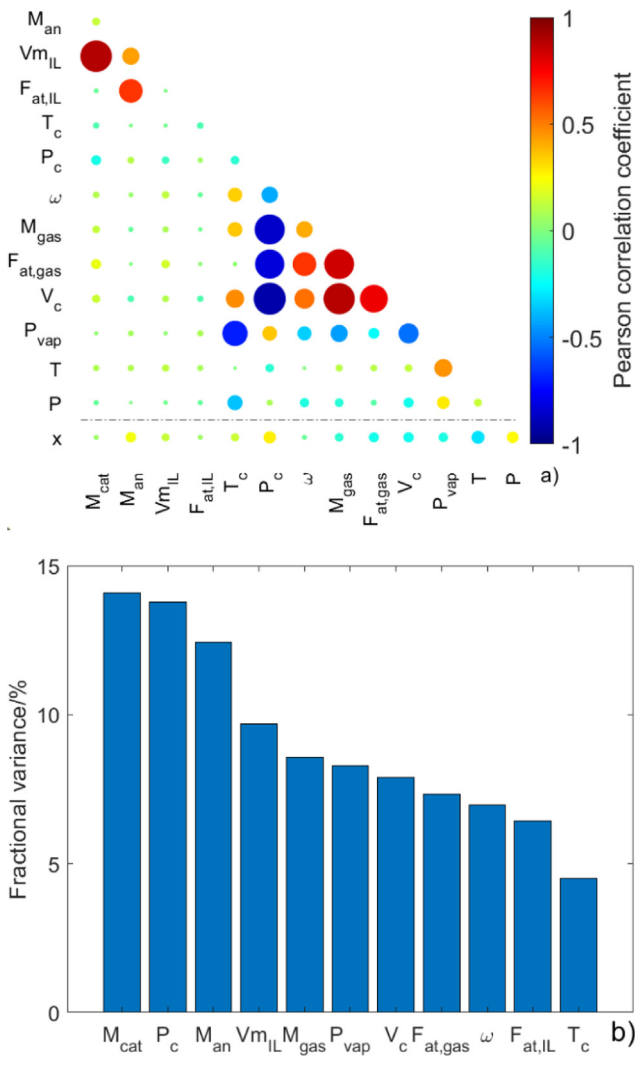

Fig. 1. (a) Pearson correlation coefficients between the input variables and the output variable (x, molar fraction of gas absorbed in the IL). The color code and the point size are related to the magnitude of the correlation coefficient according to the scale of the right-hand side of the y-axis. (b) Fractional variance of the ILs and F-gases descriptors presented as percentage of the total variance of the input variables.

3.2. Neural network training and performance

The ANNs were trained following the methodology described in section 2.2. The considered structures consisted of three-layer networks with 1 to 10 neurons in each layer (10^3 possible combinations), and 50 networks were trained for each structure, given a total number of trained networks equal to 50000. Fig. 2 shows the overall AARD of the best ANN out of each 50 ANNs trained with the same structure. As can be seen, increasing the number of neurons in the first and third layers reduces the AARD significantly, while the number of neurons in the second layer has a lower effect on the performance function.

The final structure of the ANN was selected in a point where increasing the number of neurons did not improve the performance significantly. Although it is possible to further reduce the AARD of the ANN, it may incur in overfitting derived from using too many parameters. The resulting ANN has a structure of 10, 4, and 5 neurons in the first, second, and third layer, respectively. Observing Fig. 2, it can be seen that increasing the number of neurons in the first layer has an important effect on the resulting AARD, so using the maximum limit of neurons allowed in this layer was expected. For the second and third layers, the AARD surface flattens, so there is no significant advantage in using more than 4 and 5 neurons, respectively, to obtain accurate results. Table 2 shows the performance indicators for the test set using this net-

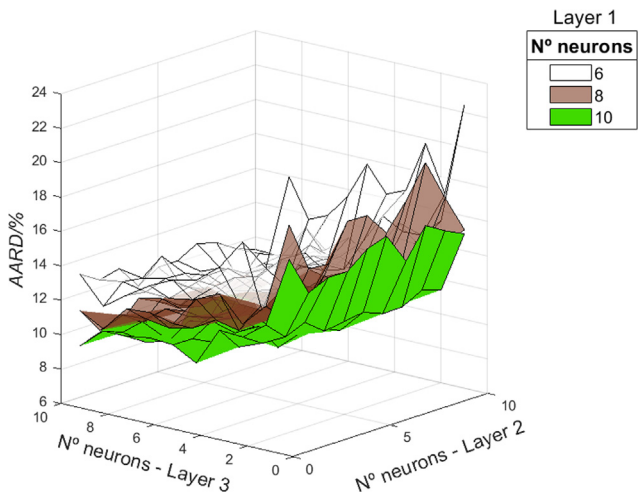

Fig. 2. Minimum AARD achieved for different number of neurons in each of the three layers of the ANN.

Table 2
Performance indicators for the neural network trained to predict the solubility of F-gases in ILs.

Indicator	Database	Train set	Validation set	Test set
AARD/%	10.93	10.39	10.98	13.41
MAE	0.014	0.014	0.014	0.015
RMSE	0.028	0.028	0.026	0.028

work. As expected, minimizing the AARD performance function was a useful strategy to obtain errors below 15% for the train, validation, and test sets and achieve an overall AARD of 10.93%, while the MAE and RMSE are very low and kept almost constant for every set. The comparison between experimental and ANN solubilities is shown in Fig. 3, showing that most of the data can be well reproduced using the developed model.

An analysis *a posteriori* of the influence of the variables on the output provides meaningful insights of the systems subject to study. To that end, we present here an analysis performed using the Partial Derivatives (PaD) method, as it was found to be the most useful approach to study the contribution of the inputs to the ANN output [52]. As its name indicates, the PaD method consists in calculating the partial derivatives of the output with respect to the input variables. The resulting relative contribution (%) of each input on the F-gas solubility is presented in Fig. 4. Moreover, this method yields a set of graphs that enables direct access to the influence of the input variable on the output, which are presented in Figures S2 (relating the derivatives to their corresponding input) and Figure S3 (relating the derivatives to the resulting molar fraction of absorbed gas in the IL solvent) in the Supplementary Information. Figure S2 and S3 show that the derivatives with respect to every variable take both positive and negative values where linear relationships between the derivatives and the molar fraction can be seen, although they are fuzzy, and no obvious trends can be inferred.

Fig. 4 shows that the critical temperature of the gas is the input variable having the highest impact (61.2%) on the calculated absorbed gas molar fraction. This result reinforces the importance of the empirical trend found in previous works pointing to the strong relationship observed between the Henry's law constants for the absorption of different F-gases in a certain IL and the critical temperature of the F-gas being absorbed [10,53]. The following two variables in order of importance are also gas-related properties: the critical volume and the number of fluorine atoms. The relevance of the critical volume of the gas (13.3%) shows that the size of the solute is a determining factor in the prediction of the solubility, i.e., the lower the critical volume, the higher the solubility (for that reason, in Figures S2 and S3, the derivative of the output with respect to critical volume is mostly negative). Similarly, there is an important contribution (6.4%) of the number of fluorine atoms of the gas molecule (Fig. 4) that indicates that it is a relevant descriptor for the prediction of the molar fraction of F-gas absorbed in ILs. Interestingly, the relative contribution of the critical pressure (3.7%) only represents the fourth most important gas feature, whereas this property exhibited one of the highest correlation coefficients to the solubility and was ranked as the gas feature with the highest importance in Fig. 1. This fact clearly shows that an analysis of the correlation coefficients is not enough to infer the influence of the input variables on the ANN output, and highlights the importance of evaluating the relative contribution of each input variable after obtaining the parameters of the final ANN.

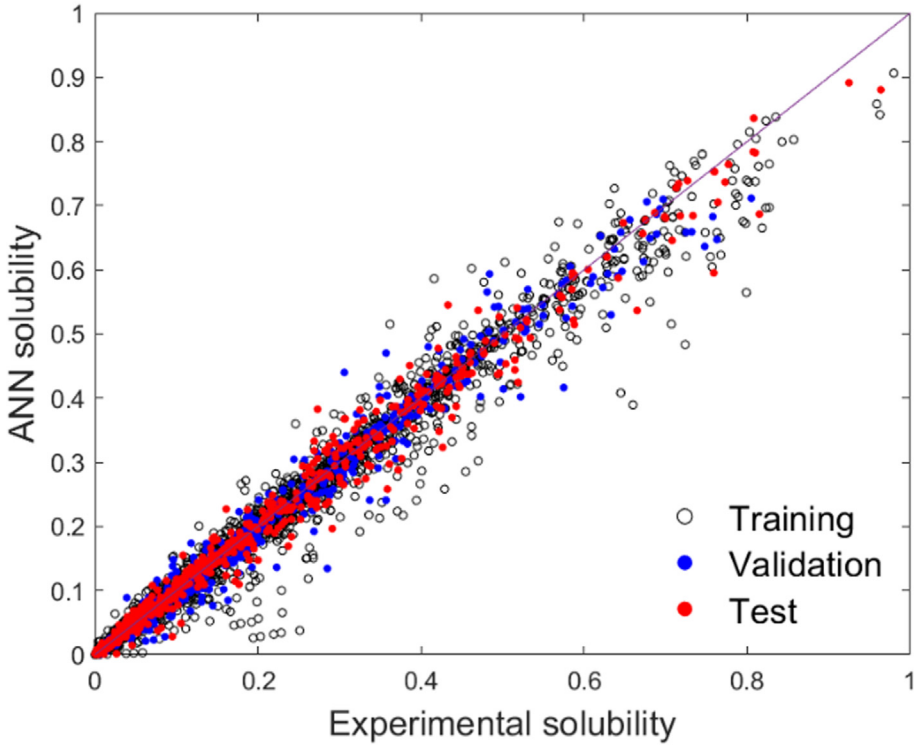

Fig. 3. Comparison between the experimental and ANN solubilities for the training, validation and test sets.

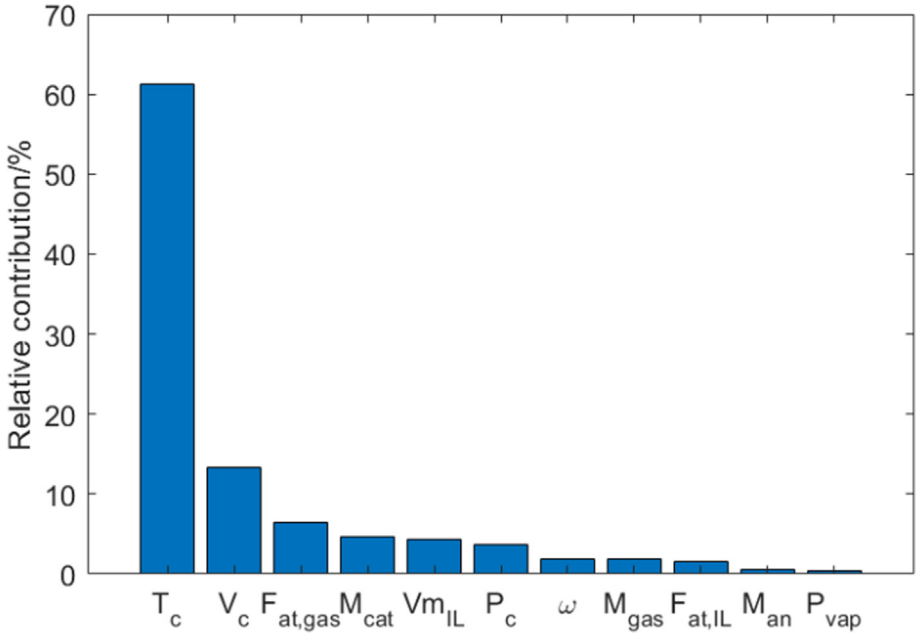

Fig. 4. Contribution of the input variables to the F-gas solubility in ILs for the three-layer 10-4-5 ANN calculated with the PaD method.

Regarding the IL features, the two properties with the highest importance are the cation molar mass (4.7%) and the IL molar volume (4.4%). This result also confirms our previous analysis of the F-gas solubility using the Regular Solution Theory [10], according to which the ILs with lower molar volume have lower absorption capacities towards F-gases. The rest of the variables related to the IL properties do not have strong contributions on the F-gas solubility, as shown in Fig. 4.

Future extensions of this ANN to expand its domain of application should consider mainly the gas critical properties and the number of fluorine atoms in the gas molecule, as well as the IL molar mass and volume. A successful extension should also include properties related to polarity. For example, including the dipole moment of the gases could be beneficial to allow the ANN to distinguish the behavior of F-gases from apolar molecules like hydrocarbons. However, including information on the polarity of the ILs would be more difficult, as IL solvents are segregated in polar and apolar domains [54,55]. Maybe using solvatochromic properties like the Kamlet-Taft parameters would help in this regard as they describe the dipolarity/polarizability, and hydrogen bond acidity and basicity [56], but currently there are not enough data available to cover all the ILs considered in this database. Additionally, molecular modeling and machine learning can be modeled by using advanced molecular models and equations of state to generate descriptors of the molecules to be fed to the machine learning algorithms [8,28]. For example, the newly proposed quantum chemical parameters referred to as ionic polarity index could be applied to describe IL polarity based on the ion charge and average surface potential [57].

Fig. 5 presents the performance of the ANN to predict the solubility in ILs of each of the 24 F–gases included in the network training in terms of both the AARD and MAE. The F-gases in Fig. 5 are grouped in four families: first, the gases that cannot be used in current equipment because they were phased out, second, the PFCs, used in ultra-low temperature applications and characterized because they do not contain hydrogen atoms, third, the HFCs that are currently predominant in installed RAC equipment, and last, the HFOs that are now entering the RAC market. As can be seen, the ANN results are accurate for predicting the solubility in ILs of the HFCs R-32, R-134a, and the HFOs R-1234yf, and R-1234ze(E), the most extended gases in current refrigerant mixtures, with AARD < 10% except for R-134a, for which the ARRD is 12%. Also, the HCFC R-22, that is present in end-of-life RAC equipment, is predicted accurately by the ANN. The high error observed in the prediction of R-23 and R-41 solubilities may be due to the fact that these F-gases are the only ones studied with ammonium-based ILs that contain carboxylate anions. As mentioned earlier, carboxylate anions are suspected to have strong polar interactions with R-134a and R-125, and they may be interacting with R-41 and R-23 too, but there is not enough empirical information available in this regard. The training of an enhanced predictive model would need expanding the dataset to include more examples of these ILs and studying the nature of the interaction between them and F-gases. With respect to R-125, a low sorbing gas, the prediction is good despite the high AARD value observed. This value is related to some experimental points with very low solubility of this gas, so that the relative error is magnified as a result of dividing by near-zero values. In the case of R-125, the good performance of the ANN is depicted by the MAE, which is only 0.020, very similar to the MAE of the calculated solubilities of a highly soluble gas like R-32.

3.3. Predictive capabilities

To show the predictive capabilities of the ANN, we present in this section the VLE of several F-gas/IL systems that were not included the UC-RAIL database as they have been recently published. Therefore, these data were not used for training the ANN. These data correspond mostly to HFOs, which are the new compounds of the fourth generation of refrigerants whose use is steadily increasing in the formulation of new refrigerant blends with the objective of reducing the impact of the RAC sector in the global warming. Table 3 shows that the network is predicting accurately the absorption of R-134a and R-1234ze(E), while it shows higher deviations for R-1233zd(E), for which the available dataset is small. Remarkably, the influence of the principal operation variables, temperature and pressure, are well predicted. This fact is of particular relevance for the usefulness of the ANN model, as temperature

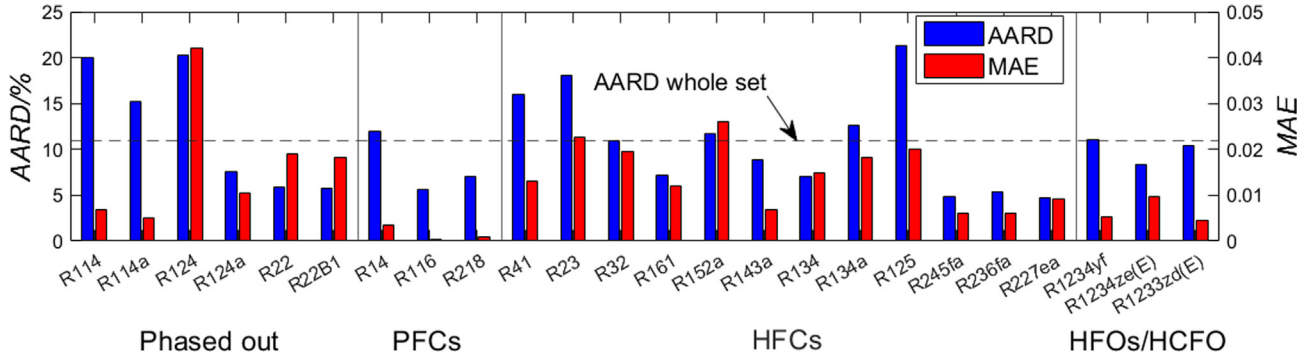

Fig. 5. AARD and MAE of the ANN as a function of the F-gas considered.

Table 3
VLE prediction of systems not included in the database. Experimental data from [58–61].

Gas + IL	*AARD/%*	*MAE*	*RMSE*
R-134a + [C_4mim][Tf_2N]	13.25	0.030	0.038
R-1234ze(E) + [P_{66614}][Cl]	10.73	0.050	0.056
R-1233zd(E) + [P_{66614}][Cl]	29.97	0.076	0.108
R-1243zf + [C_4mim][Ac]	8.49	0.007	0.009
R-1243zf + [C_4mim][OTf]	18.63	0.027	0.035
R-1243zf + [C_4mim][PF_6]	4.93	0.006	0.012

and pressure are relevant variables during the process design procedures. In fact, the chloride anion of the IL increases its solubility as mentioned in section 2.1, which results in the underprediction of the ANN. Very interestingly, the ANN predicts very accurately the solubility of R-1243zf in [C_4mim][Ac], [C_4mim][OTf], and [C_4mim][PF_6], in an ample temperature range from 283 to 343 K, as shown in Fig. 6 and Figure S4. R-1243zf is an HFO that had not been previously studied, and therefore completely unknown to the ANN, combined in the case of Fig. 6 with an IL that contains the carboxylate group. Considering the low deviation between the experimental data and predicted VLE results, the ANN proves a useful *in silico* tool to infer solubility differences between F-gases in a certain IL, thus avoiding time-consuming experimental work for the selection of task-specific ILs.

These highly accurate predictions show that the developed ANN can be reliably integrated in process design. This ANN can provide the solubility of F-gases in ILs, which can then be used to calculate Henry's law constants and ideal selectivity values for separations based in solubility differences. Furthermore, it can be included in the process design of extractive distillation columns and of new absorption refrigeration cycles where the VLE of the mixtures in the process can be calculated with this matrix multiplication procedure, easier to converge than the activity-coefficient models like NRTL.

3.4. Network parameters and easy-to-use tool

With the aim of facilitating the widespread use of the ANN presented in this work, we provide as Supplementary Material a spreadsheet containing all the ANN parameters and a calculator of F-gas solubility in ILs that implements the ANN (Fig. 7). The user simply needs to provide the 13 input parameters and the software will automatically calculate the F-gas solubility predicted by the ANN. In case the user wants to predict whole isotherms or many systems at the same time, the parameters are available in the same excel file and the formulas can be seen, so that the calculation can be easily replicated. With this, we hope to improve the user experience and favor the widespread use of the results of this article as an effective prescreening method for the abatement of high-GWP fluorinated gases using ionic liquids.

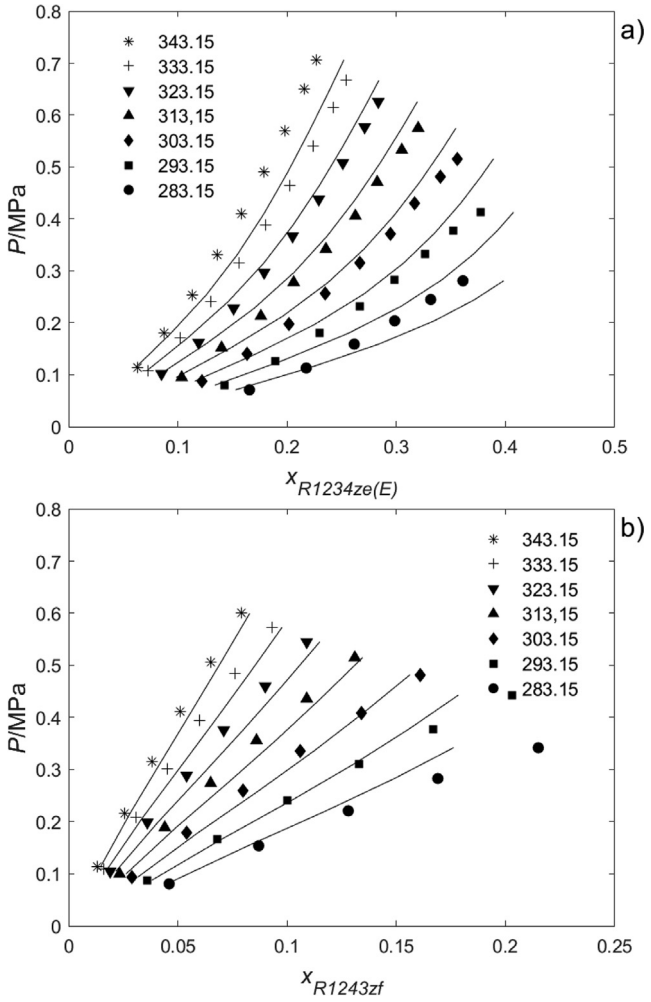

Fig. 6. Comparison between the experimental data (symbols) from references [59,60] and the ANN predictions (lines) for the systems (a) R-1234ze(E) + [P_{66614}][Cl], and (b) R-1243zf + [C_4mim][Ac].

4. Conclusions

The UC-RAIL database has been used to prepare a predictive tool for the prescreening of ionic liquids for the absorption of fluorinated refrigerant gases. This tool is based on the use of an ANN that

Introduce here the input variables		
Ionic liquid properties	M_{cat} /g·mol^{-1}	195.32
	M_{an} /g·mol^{-1}	144.97
	Vm_{IL} /cm^3·mol^{-1}	282.91
	$F_{at,IL}$	6
F-gas properties	T_c /K	367.85
	P_c /bar	33.822
	ω	0.276
	M_{gas} /g·mol^{-1}	114.04
	$F_{at,gas}$	4
	V_c /cm^3·mol^{-1}	239.81
	P_{vap} /bar	20.45
Equilibrium conditions	T/K	343.15
	P/MPa	0.4377

Prediction result	
x_{pred}	0.0693

Fig. 7. Implementation of the ANN to predict the F-gas solubility in ILs.

is fed with easily accessible pure compound properties of the solvent and solute, as well as the VLE equilibrium conditions. A total of 4396 experimental VLE points for the solubility of 24 F-gases in 52 ILs were randomly divided in training, validation, and test sets in the proportion 70/15/15 to train 50000 three-hidden-layer ANNs varying the number of neurons on each layer. Out of all the trained networks, an ANN with 10, 4, and 5 neurons in each layer was selected due to its satisfying accuracy and good predictive properties, with an overall AARD of 10.93%, and low values for the MAE and RMSE (0.014 and 0.028, respectively). Using the AARD as the objective function made possible obtaining good predictions for both high- and low-soluble refrigerant gases. Also, the relative importance of the selected inputs in the final predicted molar fraction value was evaluated, showing that the critical temperature and volume and the number of fluorine atoms of the gas have the highest contributions, followed by the IL molar volume and cation molar mass. Further refinements of this ANN to predict not only the solubility of fluorinated refrigerant gases, but also other compounds such as hydrocarbons should include information on the polarity of the solutes and solvents to improve the information introduced to the network and be able to distinguish between solute families. Nevertheless, for the purpose of fluorinated refrigerant gases, the ANN proposed in this contribution is very reliable and highly useful, as we have demonstrated predicting the vapor-liquid equilibrium of systems that are not present in the UC-RAIL database, including the gas R-1243zf, which was not present in the training whatsoever.

To facilitate the use of this ANN screening tool, we provide as Supplementary Material an easy-to-use datasheet to predict the solubility of new systems that can be applied to the design of novel separation processes aimed at the recovery of fluorinated refrigerants, with the final double purpose of increasing the share of reclaimed refrigerants in RAC equipment and contributing to the development of climate change mitigation technologies, by avoiding the release to the atmosphere of high global warming potential fluorinated gases.

CRediT authorship contribution statement

Salvador Asensio-Delgado: Conceptualization, Methodology, Software, Validation, Writing – original draft. **Fernando Pardo:** Resources, Investigation. **Gabriel Zarca:** Conceptualization, Supervision, Writing – review & editing. **Ane Urtiaga:** Conceptualization, Supervision, Writing – review & editing, Funding acquisition, Project administration.

Data availability

We have shared the data file as Supplementary Material

Declaration of Competing Interest

The authors declare that they have no known competing financial interests or personal relationships that could have appeared to influence the work reported in this paper.

Acknowledgements

This publication is a result of project PID2019-105827RB-I00 funded by MCIN/AEI/10.1039/501100011033. S. A.-D. acknowledges the FPU18/03939 grant and F.P. acknowledges the postdoctoral fellowship (FJCI-2017-32884 Juan de la Cierva Formación) awarded by the Spanish Ministry of Science and Innovation (MCIN/AEI/10.1039/501100011033).

Appendix A. Supplementary data

Supplementary data to this article can be found online at https://doi.org/10.1016/j.molliq.2022.120472.

References

[1] M.O. McLinden, C.J. Seeton, A. Pearson, New refrigerants and system configurations for vapor-compression refrigeration, Science 370 (6518) (2020) 791–796.
[2] M.O. McLinden, M.L. Huber, (R)Evolution of Refrigerants, J. Chem. Eng. Data 65 (2020) 4176–4193, https://doi.org/10.1021/acs.jced.0c00338.
[3] Y. Heredia-Aricapa, J.M. Belman-Flores, A. Mota-Babiloni, J. Serrano-Arellano, J. J. García-Pabón, Overview of low GWP mixtures for the replacement of HFC refrigerants: R134a, R404A and R410A, Int. J. Refrig. 111 (2020) 113–123, https://doi.org/10.1016/j.ijrefrig.2019.11.012.
[4] P. Purohit, L. Höglund-Isaksson, J. Dulac, N. Shah, M. Wei, P. Rafaj, W. Schöpp, Electricity savings and greenhouse gas emission reductions from global phase-down of hydrofluorocarbons, Atmos. Chem. Phys. 20 (2020) 11305–11327, https://doi.org/10.5194/acp-20-11305-2020.
[5] United Nations, Amendment to the Montreal protocol on substances that deplete the ozone layer, (2016).
[6] E.A. Heath, Amendment to the Montreal Protocol on Substances that Deplete the Ozone Layer (Kigali Amendment), Int. Leg. Mater. 56 (2017) 193–205, https://doi.org/10.1017/ilm.2016.2.
[7] European Parliament and Council, EU 517/2014, (2014) 195–230.
[8] D. Jovell, R. Gonzalez-Olmos, F. Llovell, A computational drop-in assessment of hydrofluoroethers in Organic Rankine Cycles, Energy 254 (2022) 124319.
[9] C.G. Albà, I.I.I. Alkhatib, F. Llovell, L.F. Vega, Assessment of Low Global Warming Potential Refrigerants for Drop-In Replacement by Connecting their Molecular Features to Their Performance, ACS Sustain. Chem. Eng. 9 (2021) 17034–17048, https://doi.org/10.1021/acssuschemeng.1c05985.
[10] S. Asensio-Delgado, F. Pardo, G. Zarca, A. Urtiaga, Absorption separation of fluorinated refrigerant gases with ionic liquids: Equilibrium, mass transport, and process design, Sep. Purif. Technol. 276 (2021), https://doi.org/10.1016/j.seppur.2021.119363 119363.
[11] F. Pardo, G. Zarca, A. Urtiaga, Effect of feed pressure and long-term separation performance of Pebax-ionic liquid membranes for the recovery of difluoromethane (R32) from refrigerant mixture R410A, J. Memb. Sci. 618 (2021), https://doi.org/10.1016/j.memsci.2020.118744 118744.
[12] C. Hermida-Merino, F. Pardo, G. Zarca, J.M.M. Araújo, A. Urtiaga, M.M. Piñeiro, A.B. Pereiro, Integration of stable ionic liquid-based nanofluids into polymer membranes. Part I: Membrane synthesis and characterization, Nanomaterials 11 (2021), https://doi.org/10.3390/nano11030607 607.
[13] F. Pardo, S. Gutiérrez-Hernández, C. Hermida-Merino, J.M.M. Araújo, M.M. Piñeiro, A.B. Pereiro, G. Zarca, A. Urtiaga, Integration of Stable Ionic Liquid-Based Nanofluids into Polymer Membranes. Part II: Gas Separation Properties toward Fluorinated Greenhouse Gases, Nanomaterials 11 (2021), https://doi.org/10.3390/nano11030607 582.
[14] F. Pardo, S. Gutiérrez-Hernández, G. Zarca, A. Urtiaga, Toward the recycling of low-GWP hydrofluorocarbon/hydrofluoroolefin refrigerant mixtures using composite ionic liquid-polymer membranes, ACS Sustain. Chem. Eng. 9 (2021) 7012–7021, https://doi.org/10.1021/acssuschemeng.1c00668.
[15] F. Pardo, G. Zarca, A. Urtiaga, Separation of Refrigerant Gas Mixtures Containing R32, R134a, and R1234yf through Poly(ether- block -amide)

Membranes, ACS Sustain. Chem. Eng. 8 (2020) 2548–2556, https://doi.org/10.1021/acssuschemeng.9b07195.
[16] J.E. Sosa, C. Malheiro, R.P. Ribeiro, P.J. Castro, M.M. Piñeiro, J.MM. Araújo, F. Plantier, J.PB. Mota, A.B. Pereiro, Adsorption of Fluorinated Greenhouse Gases on Activated Carbons: Evaluation of their Potential for Gas Separation, J. Chem. Technol. Biotechnol. 95 (7) (2020) 1892–1905.
[17] A.D. Yancey, S.J. Terian, B.J. Shaw, T.M. Bish, D.R. Corbin, M.B. Shiflett, A review of fluorocarbon sorption on porous materials, Microporous Mesoporous Mater. 331 (2022), https://doi.org/10.1016/j.micromeso.2021.111654 111654.
[18] D.K.J.A. Wanigarathna, J. Gao, B. Liu, Metal organic frameworks for adsorption-based separation of fluorocompounds: a review, Mater. Adv. 1 (2020) 310–320, https://doi.org/10.1039/d0ma00083c.
[19] E.A. Finberg, M.B. Shiflett, Process Designs for Separating R-410A, R-404A, and R-407C Using Extractive Distillation and Ionic Liquid Entrainers, Ind. Eng. Chem. Res. 60 (44) (2021) 16054–16067.
[20] D. Jovell, J.O. Pou, F. Llovell, R. Gonzalez-Olmos, Life Cycle Assessment of the Separation and Recycling of Fluorinated Gases Using Ionic Liquids in a Circular Economy Framework, ACS Sustain. Chem. Eng. 10 (2022) 71–80, https://doi.org/10.1021/acssuschemeng.1c04723.
[21] S. Asensio-Delgado, D. Jovell, G. Zarca, A. Urtiaga, F. Llovell, Thermodynamic and process modeling of the recovery of R410A compounds with ionic liquids, Int. J. Refrig. 118 (2020) 365–375, https://doi.org/10.1016/j.ijrefrig.2020.04.013.
[22] A. Podgoršek, J. Jacquemin, A.A.H. Pádua, M.F. Costa Gomes, Mixing Enthalpy for Binary Mixtures Containing Ionic Liquids, Chem. Rev. 116 (2016) 6075–6106, https://doi.org/10.1021/acs.chemrev.5b00379.
[23] S. Asensio-Delgado, F. Pardo, G. Zarca, A. Urtiaga, Enhanced absorption separation of hydrofluorocarbon/hydrofluoroolefin refrigerant blends using ionic liquids, Sep. Purif. Technol. 249 (2020), https://doi.org/10.1016/j.seppur.2020.117136 117136.
[24] J.E. Sosa, R. Santiago, A.E. Redondo, J. Avila, L.F. Lepre, M.F. Costa Gomes, J.M.M. Araújo, J. Palomar, A.B. Pereiro, Design of Ionic Liquids for Fluorinated Gas Absorption: COSMO-RS Selection and Solubility Experiments, Environ. Sci. Technol. 56 (2022) 5898–5909, https://doi.org/10.1021/acs.est.2c00051.
[25] S. Asensio-Delgado, M. Viar, F. Pardo, G. Zarca, A. Urtiaga, Gas solubility and diffusivity of hydrofluorocarbons and hydrofluoroolefins in cyanide-based ionic liquids for the separation of refrigerant mixtures, Fluid Phase Equilib. 549 (2021), https://doi.org/10.1016/j.fluid.2021.113210 113210.
[26] H. Qin, J. Cheng, H. Yu, T. Zhou, Z. Song, Hierarchical Ionic Liquid Screening Integrating COSMO-RS and Aspen Plus for Selective Recovery of Hydrofluorocarbons and Hydrofluoroolefins from a Refrigerant Blend, Ind. Eng. Chem. Res. 61 (11) (2022) 4083–4094.
[27] J.M. Asensio-Delgado, S. Asensio-Delgado, G. Zarca, A. Urtiaga, Analysis of hybrid compression absorption refrigeration using low-GWP HFC or HFO/ionic liquid working pairs, Int. J. Refrig. 134 (2022) 232–241, https://doi.org/10.1016/j.ijrefrig.2021.11.013.
[28] I.I.I. Alkhatib, C.G. Albà, A.S. Darwish, F. Llovell, L.F. Vega, Searching for Sustainable Refrigerants by Bridging Molecular Modeling with Machine Learning, Ind. Eng. Chem. Res. 61 (21) (2022) 7414–7429.
[29] S. Koutsoukos, F. Philippi, F. Malaret, T. Welton, A review on machine learning algorithms for the ionic liquid chemical space, Chem. Sci. 12 (2021) 6820–6843, https://doi.org/10.1039/d1sc01000j.
[30] Y. Zhao, X. Zhang, L. Deng, S. Zhang, Prediction of viscosity of imidazolium-based ionic liquids using MLR and SVM algorithms, Comput. Chem. Eng. 92 (2016) 37–42, https://doi.org/10.1016/j.compchemeng.2016.04.035.
[31] K. Wang, H. Xu, C. Yang, T. Qiu, Machine learning-based ionic liquids design and process simulation for CO2 separation from flue gas, Green, Energy Environ. 6 (2021) 432–443, https://doi.org/10.1016/j.gee.2020.12.019.
[32] M. Mesbah, S. Shahsavari, E. Soroush, N. Rahaei, M. Rezakazemi, Accurate prediction of miscibility of CO2 and supercritical CO2 in ionic liquids using machine learning, J. CO2 Util. 25 (2018) 99–107, https://doi.org/10.1016/j.jcou.2018.03.004.
[33] A. Baghban, M.A. Ahmadi, B.H. Shahraki, Prediction carbon dioxide solubility in presence of various ionic liquids using computational intelligence approaches, J. Supercrit. Fluids. 98 (2015) 50–64, https://doi.org/10.1016/j.supflu.2015.01.002.
[34] I. Mehraein, S. Riahi, The QSPR models to predict the solubility of CO2 in ionic liquids based on least-squares support vector machines and genetic algorithm-multi linear regression, J. Mol. Liq. 225 (2017) 521–530, https://doi.org/10.1016/j.molliq.2016.10.133.
[35] Z. Song, H. Shi, X. Zhang, T. Zhou, Prediction of CO2 solubility in ionic liquids using machine learning methods, Chem. Eng. Sci. 223 (2020), https://doi.org/10.1016/j.ces.2020.115752 115752.
[36] H. Feng, P. Zhang, W. Qin, W. Wang, H. Wang, Estimation of solubility of acid gases in ionic liquids using different machine learning methods, J. Mol. Liq. 349 (2022), https://doi.org/10.1016/j.molliq.2021.118413 118413.
[37] M. Nait Amar, M.A. Ghriga, H. Ouaer, On the evaluation of solubility of hydrogen sulfide in ionic liquids using advanced committee machine intelligent systems, J. Taiwan Inst. Chem. Eng. 118 (2021) 159–168, https://doi.org/10.1016/j.jtice.2021.01.007.
[38] Y. Zhao, J. Gao, Y. Huang, R.M. Afzal, X. Zhang, S. Zhang, Predicting H2S solubility in ionic liquids by the quantitative structure-property relationship method using: S σ-profile molecular descriptors, RSC Adv. 6 (2016) 70405–70413, https://doi.org/10.1039/c6ra15429h.
[39] C.A. Faúndez, R.A. Campusano, J.O. Valderrama, Misleading results on the use of artificial neural networks for correlating and predicting properties of fluids. A case on the solubility of refrigerant R-32 in ionic liquids, J. Mol. Liq. 298 (2020) 112009.
[40] E.N. Fierro, C.A. Faúndez, A.S. Muñoz, Influence of thermodynamically inconsistent data on modeling the solubilities of refrigerants in ionic liquids using an artificial neural network, J. Mol. Liq. 337 (2021), https://doi.org/10.1016/j.molliq.2021.116417 116417.
[41] C.C. Aggarwal, Neural Networks and Deep Learning, 2018. https://doi.org/10.1007/978-3-319-94463-0.
[42] A.R.C. Morais, A.N. Harders, K.R. Baca, G.M. Olson, B. Befort, A.W. Dowling, E.J. Maginn, M.B. Shiflett, Phase Equilibria, Diffusivities, and Equation of State Modeling of HFC-32 and HFC-125 in Imidazolium- based Ionic Liquids for the Separation of R-410A, Ind. Eng. Chem. Res. 59 (2020) 18222–18235, https://doi.org/10.1021/acs.iecr.0c02820.
[43] J.E. Sosa, R.P.P.L. Ribeiro, P.J. Castro, J.P.B. Mota, J.M.M. Araújo, A.B. Pereiro, Absorption of Fluorinated Greenhouse Gases Using Fluorinated Ionic Liquids, Ind. Eng. Chem. Res. 58 (2019) 20769–20778, https://doi.org/10.1021/acs.iecr.9b04648.
[44] M.S. Shannon, J.E. Bara, Reactive and Reversible Ionic Liquids for CO2 Capture and Acid Gas Removal, Sep. Sci. Technol. 47 (2012) 178–188, https://doi.org/10.1080/01496395.2011.630055.
[45] M. Kuhn, K. Johnson, Applied predictive modeling, Springer Science+Business Media, New York (2013), https://doi.org/10.1007/978-1-4614-6849-3.
[46] J. Li, L. Pan, M. Suvarna, X. Wang, Machine learning aided supercritical water gasification for H2-rich syngas production with process optimization and catalyst screening, Chem. Eng. J. 426 (2021), https://doi.org/10.1016/j.cej.2021.131285 131285.
[47] D. Serrano, D. Castelló, Tar prediction in bubbling fluidized bed gasification through artificial neural networks, Chem. Eng. J. 402 (2020) 126229.
[48] A. Tarafdar, N.C. Shahi, A. Singh, R. Sirohi, Artificial Neural Network Modeling of Water Activity: a Low Energy Approach to Freeze Drying, Food Bioprocess Technol. 11 (2018) 164–171, https://doi.org/10.1007/s11947-017-2002-4.
[49] I.H. Bell, J. Wronski, S. Quoilin, V. Lemort, Pure and Pseudo-pure Fluid Thermophysical Property Evaluation and the Open-Source Thermophysical Property Library CoolProp, Ind. Eng. Chem. Res. 53 (2014) 2498–2508, https://doi.org/10.1021/ie4033999.
[50] B.E. Poling, J.M. Prausnitz, J.P. O'Connell, The Properties of Gases and Liquids, fifth ed., McGraw-Hill Education, New York, USA, 2001.
[51] C. Albon, Machine Learning with Python Cookbook, O'Reilly Media Inc, Sebastopol, CA, 2018.
[52] M. Gevrey, I. Dimopoulos, S. Lek, Review and comparison of methods to study the contribution of variables in artificial neural network models, Ecol. Modell. 160 (2003) 249–264, https://doi.org/10.1016/S0304-3800(02)00257-0.
[53] M.B. Shiflett, A. Yokozeki, Gaseous Absorption of Fluoromethane, Fluoroethane, and 1,1,2,2-Tetrafluoroethane in 1-Butyl-3-Methylimidazolium Hexafluorophosphate, Ind. Eng. Chem. Res. 45 (2006) 6375–6382, https://doi.org/10.1021/ie060192s.
[54] K. Shimizu, M.F. Costa Gomes, A.A.H. Pádua, L.P.N. Rebelo, J.N. Canongia Lopes, Three commentaries on the nano-segregated structure of ionic liquids, J. Mol. Struct. THEOCHEM. 946 (2010) 70–76, https://doi.org/10.1016/j.theochem.2009.11.034.
[55] M.L. Ferreira, J.M.M. Araújo, A.B. Pereiro, L.F. Vega, Insights into the influence of the molecular structures of fluorinated ionic liquids on their thermophysical properties. A soft-SAFT based approach, Phys. Chem. Chem. Phys. 21 (2019) 6362–6380, https://doi.org/10.1039/c8cp07522k.
[56] S. Spange, R. Lungwitz, A. Schade, Correlation of molecular structure and polarity of ionic liquids, J. Mol. Liq. 192 (2014) 137–143, https://doi.org/10.1016/j.molliq.2013.06.016.
[57] X. Liu, K.E. O'Harra, J.E. Bara, C.H. Turner, Solubility Behavior of CO2in Ionic Liquids Based on Ionic Polarity Index Analyses, J. Phys. Chem. B. 125 (2021) 3665–3676, https://doi.org/10.1021/acs.jpcb.1c01508.
[58] T. Esaki, N. Kobayashi, H. Uchiyama, Y. Matsukuma, Characteristics of Absorption Equilibrium with HFC-134a and an Ionic Liquid Pair, J. Mater. Sci. Chem. Eng. 07 (2019) 65–78, https://doi.org/10.4236/msce.2019.73006.
[59] X. Jia, H. Wang, X. Wang, Solubility measurement, modeling and mixing thermodynamic properties of R1243zf and R600a in [BMIM][Ac], J. Chem. Thermodyn. 164 (2022), https://doi.org/10.1016/j.jct.2021.106637 106637.
[60] T. Jiang, X. Meng, Y. Sun, L. Jin, Q. Wei, J. Wang, X. Wang, M. He, Absorption behavior for R1234ze(E) and R1233zd(E) in [P66614][Cl] as Working Fluids in Absorption Refrigeration Systems, Int. J. Refrig. In press 131 (2021) 178–185.
[61] X. Jia, W. Dou, X. Wang, Solubility determination and mixing thermodynamic properties of R1243zf in two 1-butyl-3-methyl-imidazolium based ionic liquids, J. Mol. Liq. 364 (2022), https://doi.org/10.1016/j.molliq.2022.120031 120031.